Received: 14 February 2019 | Revised: 25 July 2019 | Accepted: 16 September 2019

DOI: 10.1002/acm2.12744

RADIATION ONCOLOGY PHYSICS

WILEY

Two-dimensional solid-state array detectors: A technique for *in vivo* dose verification in a variable effective area

Kananan Utitsarn[1,2] | Giordano Biasi[1] | Nauljun Stansook[1,3] | Ziyad A. Alrowaili[1,4] | Marco Petasecca[1] | Martin Carolan[5] | Vladimir L. Perevertaylo[6] | Wolfgang A. Tomé[7] | Tomas Kron[1,8,9] | Michael L. F. Lerch[1] | Anatoly B. Rosenfeld[1]

[1]Centre for Medical Radiation Physics (CMRP), University of Wollongong, Wollongong, NSW, Australia

[2]Department of Medical Services, Lopburi Cancer Hospital, Lopburi, Thailand

[3]Department of Radiology, Faculty of Medicine, Mahidol University, Bangkok, Thailand

[4]Physics Department, College of Science, Jouf University, Sakaka, Saudi Arabia

[5]Illawarra Cancer Care Centre (ICCC), Wollongong Hospital, Wollongong, NSW, Australia

[6]SPA-BIT, Kiev, Ukraine

[7]Department of Radiation Oncology, Albert Einstein College of Medicine, New York City, NY, USA

[8]Department of Physical Sciences, Peter MacCallum Cancer Centre, Melbourne, Vic., Australia

[9]Sir Peter MacCallum Cancer Institute, University of Melbourne, Melbourne, Vic., Australia

Author to whom correspondence should be addressed. Giordano Biasi
E-mail: gbiasi@uow.edu.au

Funding information
This study was funded by the National Health and Medical Research Council of Australia with the Project Grant No. APP1030159.

Abstract

Purpose: We introduce a technique that employs a 2D detector in transmission mode (TM) to verify dose maps at a depth of d_{max} in Solid Water. TM measurements, when taken at a different surface-to-detector distance (SDD), allow for the area at d_{max} (in which the dose map is calculated) to be adjusted.

Methods: We considered the detector prototype "MP512" (an array of 512 diode-sensitive volumes, 2 mm spatial resolution). Measurements in transmission mode were taken at SDDs in the range from 0.3 to 24 cm. Dose mode (DM) measurements were made at d_{max} in Solid Water. We considered radiation fields in the range from 2×2 cm^2 to 10×10 cm^2, produced by 6 MV flattened photon beams; we derived a relationship between DM and TM measurements as a function of SDD and field size. The relationship was used to calculate, from TM measurements at 4 and 24 cm SDD, dose maps at d_{max} in fields of 1×1 cm^2 and 4×4 cm^2, and in IMRT fields. Calculations were cross-checked (gamma analysis) with the treatment planning system and with measurements (MP512, films, ionization chamber).

Results: In the square fields, calculations agreed with measurements to within ±2.36%. In the IMRT fields, using acceptance criteria of 3%/3 mm, 2%/2 mm, 1%/1 mm, calculations had respective gamma passing rates greater than 96.89%, 90.50%, 62.20% (for a 4 cm SSD); and greater than 97.22%, 93.80%, 59.00% (for a 24 cm SSD). Lower rates (1%/1 mm criterion) can be explained by submillimeter misalignments, dose averaging in calculations, noise artifacts in film dosimetry.

Conclusions: It is possible to perform TM measurements at the SSD which produces the best fit between the area at d_{max} in which the dose map is calculated and the size of the monitored target.

KEY WORDS
2D solid-state array detector, MP512, transmission detector, *in vivo* QA

1 | INTRODUCTION

Conformal radiotherapy techniques such as intensity-modulated radiotherapy (IMRT) and volumetric-modulated arc radiotherapy (VMAT)[1,2] require accurate verification of treatment plans. Pretreatment quality assurance (QA)[3] considers point-dose measurements performed with an ionization chamber[4] and dose distribution measurements performed with an electronic portal imaging device (EPID),[5–7] a phantom-based electronic array[8–11] or films. However, time-consuming pretreatment QA is typically considered only once before the first treatment session; potential changes or errors in all sessions will remain unaddressed and/or undetected.[12,13]

An *in vivo* verification approach validates, in real time, accuracy, and integrity of treatment plans; parameters monitored include, for instance, the output of a medical linear accelerator (linac) and the position and/or movement of the leaves of a multileaf collimator (MLC).[12–15] Solutions for *in vivo* monitoring include[16] the use of transit and transmission detectors.

Transit detectors such as EPIDs are placed so that the beam penetrates the patient first, and then the detector.[17–19] QA with transit EPIDs is challenging; their response is energy dependent and there is additional scatter from the patient; also, they are not able to discriminate between changes in signal due to changes in fluence incident on the patient from changes in signal due to anatomical variations within the patient.[20]

Transmission detectors are, instead, placed between the linac head and the patient. Commercially available options include the Device for Advanced Verification of IMRT Delivery (DAVID) system (PTW, Freiburg, Germany), a flat, multiwire transmission-type ionization chamber[21,22]; the Dolphin detector with the COMPASS software (IBA Dosimetry, Germany), which uses 1513 air-vented plane parallel ionization chambers,[23–25] the integral quality monitoring (IQM) system (iRT Systems GmbH, Koblenz, Germany), a large-area wedge ionization chamber[12,13,26,27]; the Delta[4] Discover (ScandiDos AB, Uppsala, Sweden), a 2D solid-state array.[16] Several prototypes have also been proposed in the literature, including optical attenuation-based scintillating fibers[28]; 2D solid-state arrays, such as the MP121[29,30] and the MP512.[31]

Transmission detectors allow for independent monitoring of the output of a linac, and of the position and/or movement of the leaves of an MLC.[16] However, they have limitations. Any device placed in the beam path affects beam quality and introduces beam attenuation,[12] and as such has to be modeled in the treatment planning system (TPS).[27] Also, transmission detectors may increase surface dose[16,23] and their efficacy for beam monitoring is limited by their shape, active area, and spatial resolution.

The present study introduces a novel technique for using a 2D solid-state array prototype, the MP512 (512 diode-sensitive volumes, 2 mm spatial resolution). The MP512 was used in transmission mode (TM) to verify dose maps at a depth of d_{max} in Solid Water. TM measurements were taken at different surface-to-detector distances (SDDs) in order to adjust the area at d_{max} where the dose map is calculated.

2 | MATERIALS AND METHODS

2.A | Linear accelerator and treatment planning system

All measurements were performed at the Illawarra Cancer Care Centre (Wollongong, NSW, Australia) using a Varian Clinac® iX (Varian Medical Systems, Palo Alto, CA, USA) linac equipped with a Millennium 120-MLC with leaf width at the center of 5 mm. The linac operated with a pulse frequency of 360 Hz and was calibrated to deliver 1 cGy/MU at d_{max} in water, at 100 cm source-to-surface distance (SSD). In all cases, a 6 MV flattened photon beam was used.

For all dose calculation with a TPS, and for all IMRT plans, we used the Pinnacle's adaptive convolution-superposition (CS) algorithm implemented into the Pinnacle[3] TPS version 14 (Philips Medical Systems, Eindhoven, the Netherlands). Dose calculations were performed with a grid of 2 mm. Also, clinical IMRT plans were created, within the TPS, based on computed tomography (CT) datasets of the Solid Water phantom; a SOMATOM CT Scanner (Siemens Healthineers, Erlangen, Germany), acquiring axial slices of 2 mm, was used.

2.B | The MP512 system

The MP512 is a prototype of a monolithic silicon-array detector; it was developed at the Centre for Medical Radiation Physics (University of Wollongong, NSW, Australia). The prototype has 512 diode-sensitive volumes; these have an area of 0.5×0.5 mm^2 and are uniformly distributed with a pitch of 2 mm over an active area of 52×52 mm^2. The MP512 is operated in passive mode (i.e., no external bias is applied); its associated readout electronics has a high temporal resolution (pulse-by-pulse signal acquisition).[32]

In the literature, the MP512 has been characterized as a phantom-based detector for quality assurance in modern radiotherapy; it was demonstrated to be an accurate dosimeter for the measurement of output factors, percentage depth dose distributions, and lateral-dose profiles; furthermore, its angular dependence was investigated and corrected for, making it a suitable candidate for quality assurance in arc deliveries.[33–35] The use of the MP512 as a transmission detector was also assessed.[31] In that study, it was reported that the MP512 in TM increases the surface dose by <25% for a SDD in the range from 0.3 to 18 cm, and by <5% for SDD >18 cm.[31] The transmission factor, at d_{max} depth in Solid Water, 100 cm SSD, was in the range from 1.020 to 0.997 for SDDs from 0.3 to 24 cm.[31]

2.C | Gafchromic™ EBT3 films and Farmer ionization chamber

We considered measurements with Gafchromic™ EBT3 films and with a Farmer NE2571 ionization chamber, performed under the same experimental conditions.

Films were scanned with an EPSON Expression 10000 XL flatbed scanner using a 48-bit RGB and a resolution of 72 dpi. Films

were pre- and post-scanned (24 hrs after irradiation) six times maintaining a consistent orientation and using only the last three optical density maps. Films were calibrated using absolute dose measurements with the Farmer chamber.[36] Film analysis methodology was the same as that used by Aldosari et al.[37]

2.D | Measurements in transmission mode and in dose mode

The MP512's active area was made light-tight using a black plastic sheet of thickness 80 μm. An equalization procedure, performed prior to all measurement, was used to address a nonuniformity in the integral response of the MP512's sensitive volumes.[38] Also, to convert readings to absolute dose, the MP512 was calibrated using measurements of response linearity with dose; those measurements were performed in jaws-defined fields of 10×10 cm^2, at a depth of d_{max} in Solid Water, 100 cm SSD. Delivered MUs were in the range from 1 to 1000 MU, at a fixed dose rate of 600 MU/min. The Farmer chamber was used for the absolute dose measurements at a depth of d_{max} in Solid Water.[36]

For TM measurements, the MP512 was sandwiched between two protective slabs of PMMA of thickness 3 mm. To minimize the resulting composite thickness, each slabs had an opening, centered on the axis of the MP512's active area, of 9.5×9.5 cm^2 (Figure 1). The MP512 was then lodged into a movable holder of PMMA; by moving the holder, the SDD could be varied in the range from 0.3 to 24 cm (Figure 2). The effective area (A_{eff}), at a depth of d_{max} in Solid Water, was defined as a function of SDD as:

$$A_{eff} = A_{MP512}\left(\frac{SSD + 1.5}{SSD - SDD}\right)^2, \quad (1)$$

with A_{MP512} the MP512's active area.

For dose mode (DM) measurements, the MP512 was placed at a depth of d_{max}, in Solid Water on the treatment couch. In that case, the MP512 was sandwiched between two slabs of PMMA of thickness 5 mm; the top slab had a small recess (or air gap),[39] centered on the axis of the MP512's active area, of thickness 0.5 mm. The air gap was necessary to minimize, in small radiation fields,[40] the number and size of corrections required to relate the MP512's readings to dose.[41]

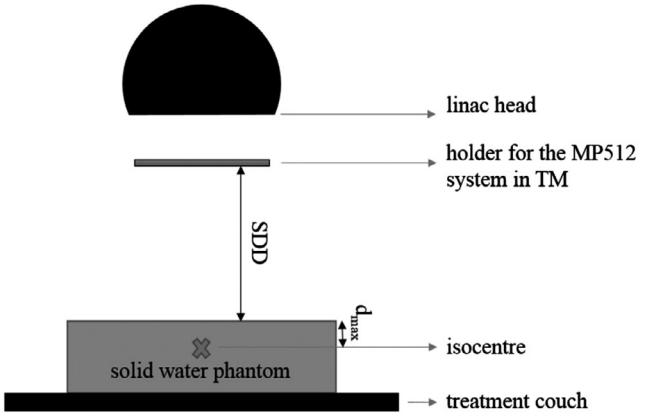

FIG. 2. Use of the MP512 system in transmission mode (not to scale).

TM and DM measurements were performed in jaws-defined static fields of 2×2 cm^2, 3×3 cm^2, 5×5 cm^2, 8×8 cm^2, and 10×10 cm^2, as defined at 100 cm SSD, delivering 200 MU at 600 MU/min. All measurements were repeated three times to minimize random uncertainties and errors were calculated as one standard deviation. In all fields, the ratio between DM measurements and TM measurements, as a function of SDD, was fit using the least square method.

2.E | Dose calculations in static square fields and IMRT fields

The response of the MP512 in TM was measured in static fields of 1×1 cm^2 and 4×4 cm^2, at 4 and 24 cm SDD. In each of these

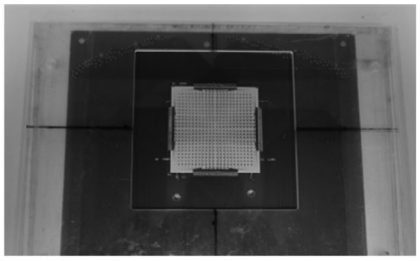

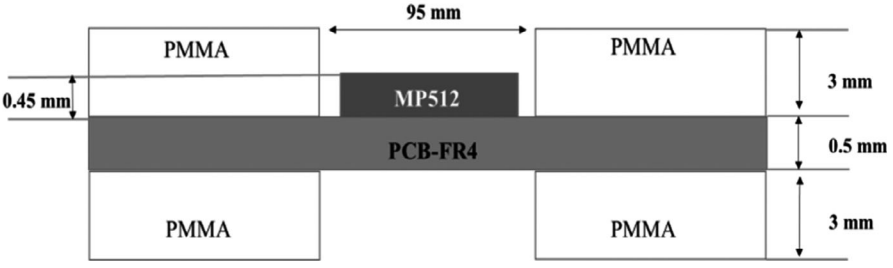

FIG. 1. (Upper panel) A snapshot of the active area of the MP512 and protective PMMA slabs. (Lower panel) A schematic of the packaging of the MP512 system, with the MP512 active area proper, upper and lower PMMA protective slabs, and the PCB-FR4 board on which the detector is wire bounded for signal readout.

fields, the response of the MP512 in DM at d_{max} was then calculated using the relationship between DM and TM measurements derived as described in the previous section. Note that these fields were not part of those used to obtain the relationship in the first place. As the field of 1×1 cm^2 was smaller than the smallest field used for the fit, the calculated response in DM was extrapolated. The response in DM in the square field of 4×4 cm^2 was calculated by interpolation. Calculated responses in DM were then compared with responses in DM measured with the MP512 itself, with Gafchromic™ EBT3 films and with a Farmer ionization chamber.

Additionally, the response of the MP512 in TM was measured at 4 and 24 cm SDD in clinical IMRT fields; these fields were delivered with a treatment plan used to treat a malignant base of skull chordoma. The step-and-shoot plan, consisting of six static fields defined by the MLC, delivered a nominal dose 1.8 Gy per fraction to a gross tumor volume (GTV) of 12.40 cm^3. All fields were delivered with the gantry at 0° (incident beam perpendicular to the active area of the MP512) to rule out angular dependence effects on the response.[35,42] Equivalent square fields (A_{eq}) of IMRT fields were calculated using[43]:

$$A_{eq} = \frac{2xy}{x+y} \quad (2)$$

As above, in each of these fields, the response of the MP512 in DM at d_{max} was then calculated using the relationship between DM and TM measurements. Calculated dose distributions were compared with TPS calculations and with DM measurements with the MP512 itself and with Gafchromic™ EBT3 films. The comparison was performed with a gamma index analysis with the following acceptance criteria: 1%/1 mm, 2%/2 mm, and 3%/3 mm; a global threshold of 10% was applied.

3 | RESULTS

3.A | Measurements in transmission mode and in dose mode

Figure 3 shows ratios between DM and TM measurements with the central sensitive volume of the MP512. Ratios, a function of field size and SDD, were fit; corresponding slopes (M) and axis intercepts (B_{A0}) are in Table 1. It was observed that M depends weakly on field size. Based on this result, it was chosen to work with its value averaged across all considered fields. Also, to compute M and B_{A0}, we operated on the central sensitive volume first; we then repeated the procedure for all other sensitive volumes — all volumes had values of M and B_{A0} in agreement to within 1.79%.

Using the averaged M (0.0196) and the B_{A0} value corresponding to any given field size, the dose in DM at d_{max} was calculated using the TM measurement at a given SDD as:

$$DM = TM_{SDD} \times (B_{A0} - M \times SDD) \quad (3)$$

For an arbitrary radiation field of area A, B_{A0} could be found from the piecewise polynomial fit (adjusted regression coefficient $R^2 = 1$) (Figure 4):

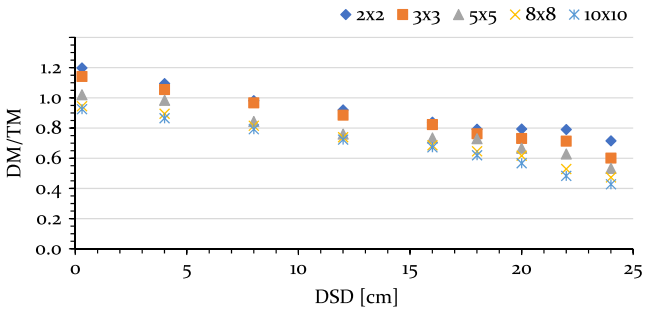

FIG. 3. Central sensitive volume of the MP512: ratio of dose mode measurements to transmission mode measurements as a function of surface-to-detector distance, for all considered square fields. Error bars did not exceed symbol size.

TABLE 1 Central sensitive volume of the MP512: slope (M) and axis intercept (B_{A0}) of the ratio of dose mode measurements to transmission mode measurements, for all considered square fields; absolute values.

	Square field, side [cm]				
Parameter	2	3	5	8	10
M	0.020	0.021	0.018	0.019	0.020
B_{Ao}	1.165	1.144	1.028	0.969	0.953

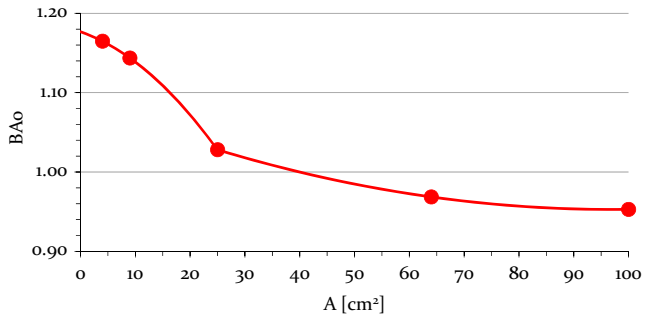

FIG. 4. Ratio of measurements in dose mode at d_{max} to measurements in transmission mode: B_{Ao} as a function of radiation field area A. Error bars did not exceed symbol size.

$$B_{Ao} = -0.000142 \times A^2 - 0.002392 \times A + 1.176743, \quad (4)$$

for 0 cm^2 ≤ A ≤ 25 cm^2, and

$$B_{Ao} = 0.000015 \times A^2 - 0.002822 \times A + 1.089544, \quad (5)$$

for 25 cm^2 ≤ A ≤ 100 cm^2.

3.B | Dose calculations in regular static fields and IMRT fields

B_{A0} values relative to static fields of 1×1 cm^2 and 4×4 cm^2 side, and to IMRT fields, were calculated using Equations 4 and 5.

Table 2 shows calculated dose at d_{max} (using TM measurements at 4 and 24 cm SDD) along with corresponding TPS calculations and DM measurements performed with the MP512 itself, with Gafchromic™ EBT3 films, and with a Farmer ionization chamber.

Table 3 shows gamma passing rates (%GP) between calculated dose distributions for IMRT fields at d_{max} (using TM measurements at 4 and 24 cm SDD) and corresponding TPS calculations and DM measurements performed with the MP512 itself and Gafchromic™ EBT3 films.

4 | DISCUSSION

A relationship was derived (Equation 3) for calculating dose, at a depth of d_{max}, by using TM measurements with the MP512 at a given SDD, in any given field. The relationship was used to calculate dose at d_{max} by using TM measurements, at 4 and 24 cm SSD, in static fields of 1×1 cm^2 and 4×4 cm^2. Calculations agreed to within ±2.36% (mean difference 1.43%) with TPS calculations and DM measurements performed with the MP512 itself, with Gafchromic™ EBT3 films, and with a Farmer ionization chamber.

The relationship was also used to calculate dose at d_{max} by using TM measurements, at 4–24 cm SSD, in step-and-shoot clinical IMRT fields. Calculated dose maps had %GP, when compared with TPS calculations and film dosimetry, greater than 96.89%, 90.50%, 62.20% (SDD 4 cm) and greater than 97.22%, 93.80%, 59.00% (SDD 24 cm), using acceptance criteria of 3%/3 mm, 2%/2 mm, and 1%/1 mm, respectively.

In the clinical practice, dose distributions are typically compared using gamma index analysis,[44–46] with a clinically significant acceptance criterion of a 3% dose difference (%DD) and 3 mm distance-to-agreement (DTA).[1,47,48] In the present study, more stringent criteria were also considered for completeness. Our dose calculations had significantly lower %GP when considering a 1%/1 mm acceptance criterion. This result can be explained by factors such as sub-millimeter misalignments in TM detector positioning, dose averaging in TPS calculations over a 2 mm grid, noise artifacts created by film heterogeneities, as well as handling and scanning procedures. Misleading results from the gamma index analysis may also originate from the use of detectors with a resolution not appropriate for the selected acceptance criterion.[49] The use of a 2D solid-state detector prototype in TM with a higher resolution than the MP512, such as the Octa (0.3 mm),[50,51] would help to shed light.

Note that, in the present study, the MP512 was not modeled into the TPS. Its transmission factor was reported to be in the range from 1.020 to 0.997 for SDDs from 0.3 to 24 cm.[31] However, if clinical use will be considered, it is suggested that transmission factor has to be adequately incorporated into a TPS.[12]

The effective area, at a depth of d_{max} in Solid Water (Equation 1), in which dose maps could be calculated based on TM measurements varied in the range from 28 cm^2 (SDD 0.3 cm) to 48.2 cm^2 (SDD 24 cm); those values reflected a MP512 having an active area of 27.04 cm^2. Depending on the clinical application, a 2D detector of larger active area may be required.

Using the MP512 in TM lodged on a holder positioned away from the linac head has the additional advantage of minimizing the contribution of scattered electrons, so that the detector response is mostly driven by the photon energy fluence, potentially simplifying 3D dose reconstructions at d_{max} in phantom.

Our study, a preliminary investigation, had the limitations of considering only 6 MV flattened photon beams, of not assessing the DM to TM ratio in fields off-axis, and of using a unique B_{A0} value for both jaws-defined and MLC-defined fields, also neglecting the influence of the backup jaws.

TABLE 2 Static square field of 1 and 4 cm side: calculated dose [Gy] at d_{max} (using transmission mode measurements at 4 and 24 cm SDD) compared with treatment planning system (TPS) calculations and dose mode measurements performed with the MP512, with films and with a Farmer ionization chamber.

Square field, side [cm]	MP512, calc.		MP512, meas.	TPS	EBT3	Farmer chamber
	4 cm SDD	24 cm SDD				
1	0.798	0.821	0.816	0.810	0.809	0.813
4	1.013	1.020	1.004	0.996	0.998	1.010

TABLE 3 Intensity-modulated radiotherapy fields: gamma evaluation for dose calculations at d_{max} (using transmission mode measurements at 4 and 24 cm SDD) and corresponding treatment planning system calculations and dose mode measurements performed with the MP512 and with films.

SDD [cm]	Acceptance criteria								
	3%/3 mm			2%/2 mm			1%/1 mm		
	MP512, calc. vs. TPS	MP512, calc. vs. EBT3	MP512, calc. vs. MP512, meas.	MP512, calc. vs. TPS	MP512, calc. vs. EBT3	MP512, calc. vs. MP512, meas.	MP512, calc. vs. TPS	MP512, calc. vs. EBT3	MP512, calc. vs. MP512, meas.
4	98.14%	96.89%	99.79%	90.50%	92.00%	98.59%	62.20%	69.40%	99.40%
24	97.22%	97.53%	99.69%	93.80%	93.80%	97.69%	59.00%	71.00%	99.00%

5 | CONCLUSION

The introduced technique uses a variable SDD for transmission mode (TM) measurements with a 2D detector. In this way, dose maps at a depth of d_{max} in Solid Water are calculated in an effective area (A_{eff}) tailored to the size of the monitored target.

When considering a gamma index analysis with a strict 1%/1 mm acceptance criterion, lower gamma passing rates (%GP) between our dose calculations and benchmarks (treatment planning system calculations, film dosimetry), which can be due to submillimeter misalignments in detector positioning or dose averaging in calculations, emphasize the importance of developing array detectors with high-spatial resolution.

This study represents a first step in the development of a real-time high-resolution 3D dose reconstruction technique based on TM measurements with the MP512 prototype.

ACKNOWLEDGEMENT

Kananan Utitsarn was supported by the Department of Medical Services, Lopburi Cancer Hospital (Lopburi, Thailand). We acknowledge the Gross Foundation (Melbourne, Australia) for financial support. We thank Todsaporn Fuangrod at the School of Medicine and Public Health, Chulabhorn Royal Academy, Bangkok, Thailand.

CONFLICTS OF INTEREST

The authors declare they have no conflict of interest.

REFERENCES

1. Ezzell GA, Burmeister JW, Dogan N, et al. IMRT commissioning: Multiple institution planning and dosimetry comparisons, a report from AAPM Task Group 119. *Med Phys*. 2009;36(11):5359–5373.
2. Bedford James L, Warrington Alan P. Commissioning of volumetric modulated arc therapy (VMAT). *Int J Radiat Oncol Biol Phys*. 2009;73(2):537–545.
3. Miften M, Olch A, Mihailidis D, et al. Tolerance limits and methodologies for IMRT measurement-based verification QA: Recommendations of AAPM Task Group No. 218. *Med Phys*. 2018;45(4):e53–e83.
4. Dong L, Antolak J, Salehpour M, et al. Patient-specific point dose measurement for IMRT monitor unit verification. *Int J Radiat Oncol Biol Phys*. 2003;56(3):867–877.
5. Bresciani S, Poli M, Miranti A, et al. Comparison of two different EPID-based solutions performing pretreatment quality assurance: 2D portal dosimetry versus 3D forward projection method. *Phys Medica*. 2018;52:65–71.
6. Blake SJ, McNamara AL, Vial P, Holloway L, Kuncic Z. Optimisation of the imaging and dosimetric characteristics of an electronic portal imaging device employing plastic scintillating fibres using Monte Carlo simulations. *Phys Med Biol*. 2014;59(22):6827–6840.
7. Agnew A, Agnew CE, Grattan MWD, Hounsell AR, McGarry CK. Monitoring daily MLC positional errors using trajectory log files and EPID measurements for IMRT and VMAT deliveries. *Phys Med Biol*. 2014;59(9):N49–N63.
8. Li G, Zhang Y, Jiang X, et al. Evaluation of the ArcCHECK QA system for IMRT and VMAT verification. *Phys Medica*. 2013;29(3):295–303.
9. Létourneau D, Gulam M, Yan D, Oldham M, Wong JW. Evaluation of a 2D diode array for IMRT quality assurance. *Radiother Oncol*. 2004;70(2):199–206.
10. Feygelman V, Forster K, Opp D, Nilsson G. Evaluation of a biplanar diode array dosimeter for quality assurance of step-and-shoot IMRT. *J Appl Clin Med Phys*. 2009;10(4):64–78.
11. Blanck O, Masi L, Chan MKH, et al. High resolution ion chamber array delivery quality assurance for robotic radiosurgery: Commissioning and validation. *Phys Medica*. 2016;32(6):838–846.
12. Casar B, Pasler M, Wegener S, et al. Influence of the integral quality monitor transmission detector on high energy photon beams: A multi-centre study. *Z Med Phys*. 2017;27(3):232–242.
13. Chang J, Heaton RK, Mahon R, et al. A method for online verification of adapted fields using an independent dose monitor. *Med Phys*. 2013;40(7):072104.
14. Wu QJ, Li T, Wu Q, Yin FF. Adaptive radiation therapy: technical components and clinical applications. *Cancer J*. 2011;17(3):182–189.
15. Mijnheer B, Beddar S, Izewska J, Reft C. *In vivo* dosimetry in external beam radiotherapy. *Med Phys*. 2013;40(7):1–19.
16. Li T, Wu QJ, Matzen T, Yin FF, O'Daniel JC. Diode-based transmission detector for IMRT delivery monitoring: A validation study. *J Appl Clin Med Phys*. 2016;17(5):235–244.
17. McDermott LN, Wendling M, Sonke JJ, van Herk M, Mijnheer BJ. Replacing pretreatment verification with *In Vivo* EPID dosimetry for prostate IMRT. *Int J Radiat Oncol Biol Phys*. 2007;67(5):1568–1577.
18. Slosarek K, Szlag M, Bekman B, Grzadziel A. EPID *in vivo* dosimetry in RapidArc technique. *Reports Pract Oncol Radiother*. 2010;15(1):8–14.
19. van Elmpt W, McDermott L, Nijsten S, Wendling M, Lambin P, Mijnheer B. A literature review of electronic portal imaging for radiotherapy dosimetry. *Radiother Oncol*. 2008;88(3):289–309.
20. Kron T, Lehmann J, Greer PB. Dosimetry of ionising radiation in modern radiation oncology. *Phys Med Biol*. 2016;61(14):R167–R205.
21. Poppe B, Thieke C, Beyer D, et al. DAVID - A translucent multi-wire transmission ionization chamber for *in vivo* verification of IMRT and conformal irradiation techniques. *Phys Med Biol*. 2006;51(5):1237–1248.
22. Poppe B, Looe HK, Chofor N, Rühmann A, Harder D, Willborn KC. Clinical performance of a transmission detector array for the permanent supervision of IMRT deliveries. *Radiother Oncol*. 2010;95(2):158–165.
23. Venkataraman S, Malkoske K, Jensen M, Nakonechny K, Asuni G, Mccurdy B. SU-FF-T-353: Influence of a novel transmission detector On 6 MV X-ray beam characteristics. *Med Phys*. 2009;36(6):2603.
24. Thoelking J, Sekar Y, Fleckenstein J, Lohr F, Wenz F, Wertz H. Characterization of a new transmission detector for patient individualized online plan verification and its influence on 6MV X-ray beam characteristics. *Z Med Phys*. 2016;26(3):200–208.
25. Gueorguiev G, Khan F, Toomeh D, et al. Clinical evaluation of a novel transmission detector for 3D quality assurance of IMRT and SBRT. *Biomed Phys Eng Express*. 2017;3(5):055010.
26. Islam MK, Norrlinger BD, Smale JR, et al. An integral quality monitoring system for real-time verification of intensity modulated radiation therapy. *Med Phys*. 2009;36(12):5420–5428.
27. Marrazzo L, Arilli C, Pasler M, et al. Real-time beam monitoring for error detection in IMRT plans and impact on dose-volume histograms: A multi-center study. *Strahlentherapie und Onkol*. 2018;194(3):243–254.
28. Goulet M, Gingras L, Beaulieu L. Real-time verification of multileaf collimator-driven radiotherapy using a novel optical attenuation-based fluence monitor. *Med Phys*. 2011;38(3):1459–1467.
29. Wong JHD, Fuduli I, Carolan MG, et al. Characterization of a novel two dimensional diode array the 'magic plate' as a radiation detector for radiation therapy treatment. *Med Phys*. 2012;39(5):2544–2558.
30. Alrowaili ZA, Lerch MLF, Petasecca M, Carolan MG, Metcalfe PE, Rosenfeld AB. Beam perturbation characteristics of a 2D

transmission silicon diode array, Magic Plate. *J Appl Clin Med Phys*. 2016;17(2):5932.
31. Utitsarn K, Alrowaili ZA, Stansook N, et al. Impact of a monolithic silicon detector operating in transmission mode on clinical photon beams. *Phys Medica*. 2017;43:114–119.
32. Fuduli I, Newall MK, Espinoza AA, et al. Multichannel data acquisition system comparison for quality assurance in external beam radiation therapy. *Radiat Meas*. 2014;71:338–341.
33. Petasecca M, Newall MK, Booth JT, et al. MagicPlate- 512: A 2D silicon detector array for quality assurance of stereotactic motion adaptive radiotherapy. *Med Phys*. 2015;42(6):2992–3004.
34. Duncan M, Newall MK, Caillet V, et al. Real-time high spatial resolution dose verification in stereotactic motion adaptive arc radiotherapy. *J Appl Clin Med Phys*. 2018;19(4):173–184.
35. Stansook N, Biasi G, Utitsarn K, et al. 2D monolithic silicon-diode array detectors in megavoltage photon beams: does the fabrication technology matter? A medical physicist's perspective. *Australas Phys Eng Sci Med*. 2019;42(2):443–451.
36. Almond PR, Biggs PJ, Coursey BM, et al. AAPM's TG-51 protocol for clinical reference dosimetry of high-energy photon and electron beams. *Med Phys*. 1999;26(9):1847–1870.
37. Aldosari AH, Petasecca M, Espinoza A, et al. A two dimensional silicon detectors array for quality assurance in stereotactic radiotherapy: MagicPlate-512. *Med Phys*. 2014;41(9):091707.
38. Biasi G, Davis J, Petasecca M, et al. On monolithic silicon array detectors for small-field photon beam dosimetry. *IEEE Trans Nucl Sci*. 2018;65(9):2640–2649.
39. Charles PH, Crowe SB, Kairn T, et al. The effect of very small air gaps on small field dosimetry. *Phys Med Biol*. 2012;57(21):6947–6960.
40. Utitsarn K, Alrowaili ZA, Stansook N, et al. The effect of an air gap on a 2D monolithic silicon detector for relative dosimetry. *J Instrum*. 2019;14(06):P06018.
41. Andreo P. The physics of small megavoltage photon beam dosimetry. *Radiother. Oncol*. 2018;126(2):205–213.
42. Stansook N, Utitsarn K, Petasecca M, et al. Technical Note: Angular dependence of a 2D monolithic silicon diode array for small field dosimetry. *Med Phys*. 2017;44(8):4313–4321.
43. Tatcher M, Bijrngard BE. Equivalent squares of irregular photon fields. *Med Phys*. 1993;20(4):1229–1232.
44. Low DA, Harms WB, Mutic S, Purdy JA. A technique for the quantitative evaluation of dose distributions. *Med Phys*. 1998;25(5):656–661.
45. Low DA, Moran JM, Dempsey JF, Dong L, Oldham M. Dosimetry tools and techniques for IMRT. *Med Phys*. 2011;38(3):1313–1338.
46. Low DA, Dempsey JF. Evaluation of the gamma dose distribution comparison method. *Med Phys*. 2003;30(9):2455–2464.
47. Pulliam K, Kerns J, Howell R, Followill D, O' Daniel J, Kry S. MO-G-BRE- 02: A survey of IMRT QA practices for more than 800 Institutions. *Med Phys*. 2014;41(6):432–432.
48. Jin X, Yan H, Han C, Zhou Y, Yi J, Xie C. Correlation between gamma index passing rate and clinical dosimetric difference for pretreatment 2D and 3D volumetric modulated arc therapy dosimetric verification. *Br J Radiol*. 2015;88(1047):20140577.
49. Woon W, Ravindran PB, Ekayanake P, Vikraman S, Lim YY, Khalid J. A study on the effect of detector resolution on gamma index passing rate for VMAT and IMRT QA. *J Appl Clin Med Phys*. 2018;19(2):230–248.
50. Biasi G, Petasecca M, Guatelli S, et al. A novel high-resolution 2D silicon array detector for small field dosimetry with FFF photon beams. *Phys Medica*. 2018;45:117–126.
51. Biasi G, Petasecca M, Guatelli S, et al. CyberKnife® fixed cone and Iris™ defined small radiation fields: Assessment with a high-resolution solid-state detector array. *J Appl Clin Med Phys*. 2018;19(5):547–557.